A Statistical Mechanics Framework for Organic Mixed Conductors: The Charge Carrier Vapor-Liquid Transition

Lukas M. Bongartz
Institute for Applied Physics, Technische Universität Dresden, Nöthnitzer Str. 61, 01187 Dresden, Germany
(Dated: September 22, 2025)

Organic mixed conductors (OMCs) are polymer semiconductors that conduct both electronic and ionic charge carriers, enabling emerging technologies in bioelectronics, neuromorphics, and thermoelectrics. The complex dynamics of OMCs, which span multiple length- and time-scales and feature strong coupling between electronic, ionic, and mass transport, set them apart from traditional semiconductors and preclude a description using conventional theory. In this Letter, we present a statistical mechanics framework to explain these collective dynamics. We model the electronic charge carrier population as a lattice gas and investigate it using Monte Carlo simulations and mean-field analysis. This minimal model exhibits a first-order phase transition analogous to a classical vapor-liquid transition, governed by temperature and chemical potential. This approach naturally explains the formation of distinct low- and high-density carrier phases and demonstrates how metastability near the phase boundary gives rise to the history-dependent characteristics observed in device operation. This work shows that the language of statistical mechanics and phase transitions is a viable tool for understanding the complex charge carrier dynamics in OMCs.

INTRODUCTION

Organic mixed conductors (OMCs) – semiconducting polymers that conduct both ions and electrons – represent a novel class of electronic materials, distinct from conventional inorganic semiconductors like silicon [1, 2]. They form the foundation for emerging technologies in bioelectronics and neuromorphic computing, often embodied in form of an organic electrochemical transistor (OECT)[3]. In this device architecture, an OMC channel is coupled to a gate electrode via an electrolyte that serves as a reservoir for mobile dopant ions.

Their operation relies on a unique set of properties that sets OECT apart from traditional semiconductor devices: charge transport is volumetric rather than confined to a two-dimensional channel; low dielectric constants amplify Coulombic interactions between charge carriers; and, crucially, doping is a dynamic process essential for device function. OMCs are frequently operated at extremely high carrier densities ($\approx 10^{20}$–$10^{21}\,\mathrm{cm}^{-3}$), orders of magnitude beyond what is typical in inorganic systems and approaching a 1:1 population of electronic charges on the molecular hosting sites[4–6]. This confluence of characteristics situates OMCs in a regime governed by non-linear, many-body, and often non-equilibrium phenomena.

The physical complexity of OMCs is tied to their disordered microstructure, which contrasts sharply with the periodic lattice of crystalline silicon and complicates the transfer of microscopic, molecular understanding to the device scale. Within the disordered matrix, electron—electron and electron-–dopant interactions become prominent[7], leading to a dynamic density of states that evolves as a function of carrier density itself[5, 8]. Traditional semiconductor theory fails in capturing these intricate dynamics. The high charge densities, in particular, necessitate the inclusion of entropic forces, which are typically negligible in traditional semiconductor physics but become dominant in driving the collective behavior of the carrier population.

A growing body of work has revealed a suite of remarkable phenomena in OMCs, often tied to a heterogeneous doping process[7, 9–11]. These studies highlight an intricate configurational landscape governed by interactions between electronic charge carriers, mobile ionic dopants, local molecular energetics, and morphology. For example, Wu et al. identified non-equilibrium, mesoscopic correlations between charge carriers on the 10-nm length scale, revealing phase separation into domains of distinct electronic character[12]. In a different system, Bongartz et al. observed persistent bistability in OECTs gated with molecular dopants, which can thermodynamically be described as a phase separation into domains of high and low doping fraction[13].

Such observations suggest the presence of collective and critical phenomena, and seem to converge on a common underlying theme: the stabilization of charge carriers through cooperative, attractive interactions that lead to phase-separated, electronically distinct domains. In this Letter, we attempt to formalize this perspective using the tools of statistical mechanics. We propose a framework that treats the population of charge carriers as a lattice gas, demonstrating that fundamental aspects of this behavior, namely the emergence of phase-separated domains and hysteretic bistability, can be understood as an analogue of a collective vapor-liquid phase transition. We proceed by first defining the system in terms of its microscopic states and interactions, and then establishing the probabilistic framework of the grand canonical ensemble that governs its quasi-equilibrium behavior on electronic timescales.

MAIN

The Lattice Gas Model

The intricate dynamics and disordered microstructure of OMCs give rise to a vast number of possible microscopic arrangements of charge carriers, known as microstates. Device operation, however, typically probes macroscopic properties, such as the total channel conductivity or impedance, which represent ensemble averages over the microscopic landscape. This perspective motivates a statistical treatment to determine the system's equilibrium properties.

We focus on the electronic subsystem residing on the molecular backbone of the polymer. This subsystem can be effectively decoupled from the bulk material due to a separation of timescales. We therefore treat the molecular backbone as a quasi-static grid of sites that hosts the carrier population. This picture directly maps onto a lattice gas model, which is mathematically equivalent to the Ising model, where each site can either be empty or occupied by a single carrier, denoted by an occupation number $n_i \in \{0, 1\}$.

Charge carriers in soft, conjugated polymers are not free electrons but quasiparticles known as polarons, where the charge is strongly coupled to local vibrations of the molecular lattice (strong electron-phonon coupling)[14]. The lattice distortion created by one polaron forms a local potential well that can be favorably occupied by a second carrier. In conjugated polymers, these carriers are not point charges but polarons delocalized over several repeat units (along the backbone and across π-π stacks), with sizable dipole moments and high polarizability. Delocalization lowers the Coulomb self-energy and enhances overlap with the same lattice relaxation, while dipolar and induced-dipole interactions provide additional short-range stabilization. These cooperative, short-range effects can outweigh the residual like-charge repulsion, motivating our central assumption of a net effective attraction. This energetic stabilization of clustered carriers is directly analogous, in spirit, to the attractive part of intermolecular potentials (e.g., Lennard-Jones) that drives the condensation of classical fluids from a vapor.

In device operation, the OMC is not an isolated system; it is in contact with a thermal environment (the 'heat bath') and a reservoir of dopant ions (the electrolyte). By the separation of timescales, the number of host sites constitutes a constant effective volume (V) for the electronic problem. The exchange of energy with the heat bath is governed by the temperature (T), while the exchange of particles (charge carriers) with the reservoir is governed by the chemical potential (μ). This perspective, allowing for particle exchange within a fixed effective volume, naturally leads to the grand canonical ensemble. For a microstate X with $N(X) = \sum_i n_i$ carriers, the probability is given by the Boltzmann distribution:

$$\mathbb{P}[X] \propto \exp\left(-\frac{E(X) - \mu N(X)}{k_{\mathrm{B}}T}\right) \tag{1}$$

where $E(X)$ is the internal energy of the microstate and $N(X) = \sum_i n_i$ is the total number of carriers. For simplicity, we set $k_{\mathrm{B}} = 1$ henceforth. $E(X)$ is defined by the Hamiltonian for our lattice gas:

$$H = -J \sum_{\langle i,j \rangle} n_i n_j \tag{2}$$

where $J > 0$ is the effective attractive interaction energy between nearest-neighbor carriers, as motivated previously. We interpret μ as a fixed reservoir parameter (control parameter) and will later connect it to the device electrochemical potential.

While the probability of a single microstate is known, the probability of an observable macrostate (e.g., one with a specific carrier density $\rho = N/V$) must also account for its degeneracy—that is, the total number of microstates, Ω, that realize it. The probability of such a macrostate is therefore proportional to the Boltzmann factor weighted by this degeneracy: $\mathbb{P}(\text{macrostate}) \propto \Omega \cdot e^{-(E-\mu N)/T}$. This degeneracy is quantified by the configurational entropy, $S = \ln \Omega$. Substituting this into the probability expression reveals the central role of the thermodynamic potential:

$$\mathbb{P}(\text{macrostate}) \propto e^{S} e^{-(E-\mu N)/T} = e^{-\Phi/T} \tag{3}$$

where the grand potential is defined as $\Phi = E - TS - \mu N = F - \mu N$, with $F = E - TS$ being the Helmholtz free energy. The system's equilibrium state is the one that maximizes this probability, which is achieved by minimizing Φ. This minimization represents the fundamental thermodynamic balance between the energetic drive for order (minimizing E), the entropic drive for disorder (maximizing S), and the coupling to the particle reservoir ($-\mu N$).

Monte Carlo Simulation

We investigate this model's equilibrium behavior using Monte Carlo simulations based on Glauber dynamics with Metropolis acceptance[15]. The algorithm repeatedly attempts to change the state of a randomly selected lattice site. A proposed flip (e.g., creating a carrier at an empty site) results in a change in the system's energy and particle number, ΔE and ΔN. The move is accepted with probability $P_{\text{accept}} = \min(1, e^{-(\Delta E - \mu \Delta N)/T})$, which ensures that the simulation correctly samples the grand canonical distribution and converges to the system's equilibrium state at fixed μ and T.

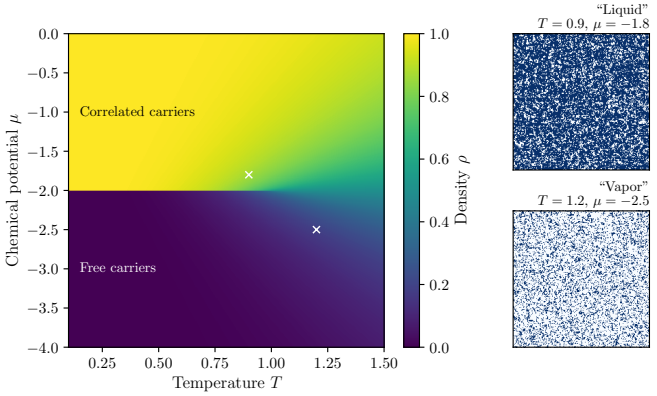

FIG. 1. Phase diagram of a lattice gas model, mapping equilibrium charge carrier density ρ against temperature T and chemical potential μ. Above a critical temperature T_c, density varies smoothly (supercritical fluid). Below T_c, a sharp, first-order phase transition occurs at $\mu_c = -2J$ (mean-field square-lattice MC, $J = 1.0$), dividing a low-density "vapor" phase (free carriers) from a high-density "liquid" phase (correlated carriers). Insets show representative simulation snapshots for each phase.

By running the simulation across a grid of parameters (T, μ), we map the system's equilibrium behavior. The primary result is a phase diagram, shown in Fig. 1, which plots the equilibrium charge carrier density ρ as a function of temperature and chemical potential. The diagram reveals two distinct regimes. At high temperatures ($T > T_c$), the carrier density changes smoothly and continuously with μ, analogous to a supercritical fluid. Below a critical temperature ($T < T_c$), however, a sharp, discontinuous jump in density appears at a critical chemical potential $\mu_c = -2J$ (the mean-field prediction for a square lattice with $J = 1$). This is a first-order phase transition, separating a low-density "vapor-like" phase of largely independent carriers from a high-density "liquid-like" phase of correlated, stabilized carriers, as shown in the insets of Fig. 1. Near this phase transition line, the system exhibits metastability; if parameters are changed such that a new phase becomes favorable, the system can remain trapped in the previous macrostate for a very long time, as an energy barrier for nucleation of the new phase must be overcome. To understand the analytical origin of this behavior, we now turn to a mean-field analysis.

Mean-Field Analysis

The regular square lattice of our simulation is a significant idealization. Real-world OMCs are high-entropy materials, whose long-chain polymers possess a vast number of conformational degrees of freedom, leading to significant structural disorder. This inherent disorder suggests that the system's collective properties are primarily governed by the average interaction a carrier experiences from its environment, rather than by the specific, local geometric arrangement of neighboring sites. To gain further analytical insight by relaxing the constraint of a specific geometry, we adopt a mean-field approximation.

In this picture, every site is assumed to interact equally with every other site, creating a fully connected network. The interaction energy of a given state now depends only on the total number of carriers, $N(X)$, not their specific arrangement. For a system with V total sites, the normalized interaction energy becomes $E(X) = -(2J/V)N(X)^2$. Substituting this into the grand canonical Boltzmann distribution gives:

$$\mathbb{P}[X] \propto \exp\left(\frac{2J}{TV}N(X)^2 + \frac{\mu}{T}N(X)\right) \tag{4}$$

This formulation connects the probability of a single microstate to its macroscopic density $\rho(X) = N(X)/V$. To find the probability of observing a macrostate with a given density ρ, we must multiply by the number of ways to arrange $N = \rho V$ carriers on V sites. This combinatorial factor gives rise to the system's entropy. A standard derivation using Stirling's approximation (see Appendix) allows us to write the probability distribution for the density ρ as:

$$\mathbb{P}[\rho] \propto \exp\left(V\left[\frac{2J\rho^2 + \mu\rho}{T} - (\rho\ln\rho + (1-\rho)\ln(1-\rho))\right]\right) \tag{5}$$

For a large system ($V \gg 1$), the probability distribution is sharply peaked around the density ρ^* that maximizes the term in the exponent. We can identify this exponent (per unit volume) as $-\phi_{T,\mu}(\rho)/T$, where $\phi_{T,\mu}(\rho) = f(\rho) - \mu\rho$ is the mean-field grand potential density, with $f(\rho) = -2J\rho^2 + T[\rho\ln\rho + (1-\rho)\ln(1-\rho)]$ being the Helmholtz free energy density. The direct relationship between the probability and the grand potential landscape is visualized in Fig. 2. The peaks in the probability distribution $\mathbb{P}[\rho]$ correspond to minima in the grand potential density $\phi_{T,\mu}(\rho)$, which represent stable or metastable equilibrium states. At high temperatures ($T > T_c$), the landscape features a single minimum that shifts continuously with μ. Below the critical temperature, however, the landscape becomes non-convex and can exhibit two distinct minima. As the chemical potential crosses the critical value μ_c, the global minimum of the grand potential jumps discontinuously from the low-density to the high-density state. This jump is the mathematical origin of the first-order phase transition.

Connection to Device Operation

Our model has so far treated the chemical potential μ as an abstract control parameter. In an operating OECT, this parameter is determined by the electrochemical environment: the electrolyte provides a reservoir of ions that

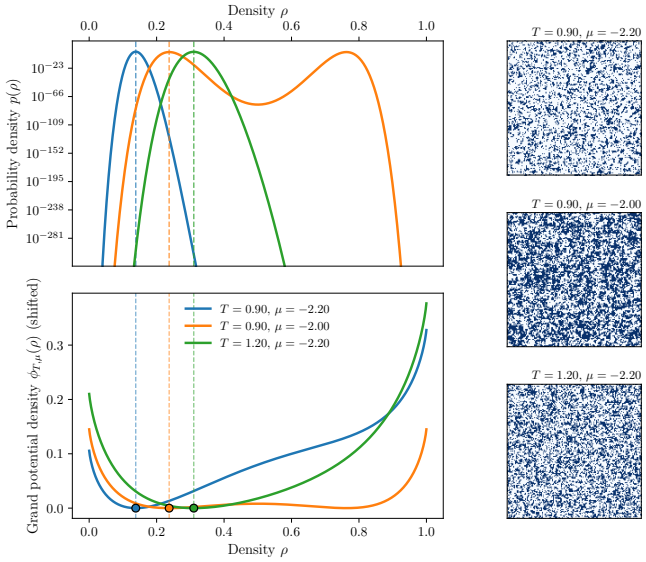

FIG. 2. Interplay of probability and grand potential in the mean-field model ($J = 1.0$). (Top) Probability density $p[\rho]$ as a function of carrier density ρ. (Bottom) The corresponding grand potential landscape, $\phi_{T,\mu}(\rho)$ (shifted vertically for clarity). The peaks in probability correspond directly to the minima in the grand potential. As the chemical potential μ increases, the most probable state (global minimum) shifts from a low-density 'vapor' phase (blue) to a high-density 'liquid' phase (green), passing through a coexistence point where both phases are equally probable (red). Insets show representative simulation snapshots for each regime.

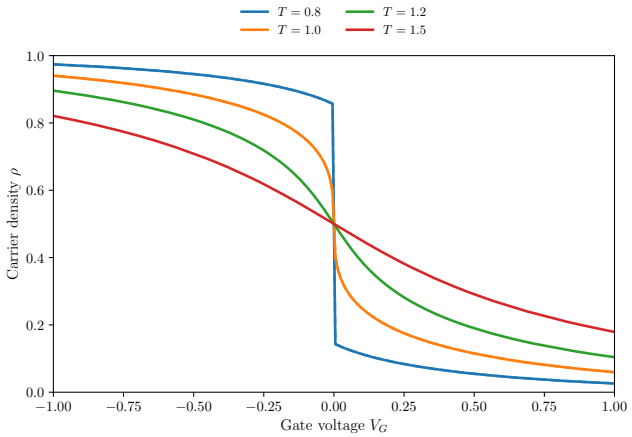

FIG. 3. Predicted transfer characteristics showing carrier density ρ as a function of gate voltage V_G for various temperatures ($J = 1$, $\mu_{\text{reservoir}} = -2.0$, $q = 1.0$). Above the critical temperature ($T = 1.2, 1.5$), the response is smooth and reversible. Below T_c ($T = 0.8, 1.0$), the first-order phase transition produces abrupt switching and hysteresis loops.

can exchange charge with the polymer channel, and the gate electrode controls the electrostatic potential of this reservoir relative to the channel.

The electrochemical potential accounts for both chemical and electrostatic contributions. For a charge carrier of charge q (with $q = -e$ for electrons, $q = +e$ for holes), the electrochemical potential is:

$$\mu_{\text{ec}} = \mu_{\text{chem}} + q\phi \tag{6}$$

where μ_{chem} is the intrinsic chemical potential and ϕ is the local electrostatic potential.

At equilibrium, carriers in the channel must have the same electrochemical potential as the reservoir. When a gate voltage V_G is applied, it shifts the channel potential relative to the electrolyte reference by $-V_G$ (assuming the electrolyte is grounded). This modifies the effective chemical potential in the grand canonical distribution:

$$\mu_{\text{eff}} = \mu_{\text{reservoir}} - qV_G \tag{7}$$

The grand canonical probability distribution thus becomes:

$$\mathbb{P}[X] \propto \exp\left(-\frac{E(X) - \mu_{\text{eff}}N(X)}{T}\right) \tag{8}$$

This framework reveals that sweeping the gate voltage is equivalent to moving through the phase diagram along the μ-axis. When V_G drives μ_{eff} across the critical value μ_c, the system undergoes a first-order phase transition between the vapor-like and liquid-like phases.

Figure 3 illustrates the predicted transfer characteristics—carrier density ρ as a function of gate voltage V_G—for several temperatures. Above the critical temperature ($T > T_c \approx 1.13$), the system exhibits smooth, reversible behavior typical of conventional transistors. Below T_c, however, the first-order phase transition manifests as abrupt switching in carrier density, accompanied by pronounced hysteresis: the forward and backward voltage sweeps trace different paths, with the system remaining trapped in metastable states. This hysteresis width decreases as temperature approaches T_c from below, consistent with the weakening of the phase transition.

Note that fundamental driving force behind this metastability is not temperature alone, but the ratio J/T (Eq. 5), which encapsulates the competition between the energetic drive for carrier coupling and the entropic drive for disorder. This behavior reflects in experimental reports. For instance, Ji et al. found an increase in hysteresis width for OECTs treated with a hydrophobic agent, which facilitates stronger electronic coupling and thus corresponds to a larger effective J [9]. Complementary to this, Bongartz et al. reported the inverse trend of shrinking hysteresis with rising temperature [13]. In general, such pronounced hysteretic phenomena are characteristic of OECT systems engineered to be in a 'strong-coupling' regime, such as those employing ionic liquids or tuned channel morphologies, where the ratio J/T is significant [10, 11].

CONCLUSION

In conclusion, we have presented a statistical mechanics framework based on a lattice gas model that describes the complex dynamics in OMCs in the high-charge carrier regime. Our results demonstrate that phenomena such as phase separation and hysteretic bistability can be understood in analogy to a collective vapor-liquid phase transition, driven by the competition between interaction energy and configurational entropy. The direct connection between gate voltage sweeps and trajectories through the thermodynamic phase diagram provides an explanation for the non-trivial transfer characteristics observed in certain devices of strong charge-carrier coupling. While this model is a significant simplification of the intricate real-world molecular and electronic interactions, its ability to capture the essential physics of a phase transition is a powerful illustration of the principle of universality: near a critical point, the qualitative macroscopic behavior (e.g., scaling laws and exponents) depends chiefly on symmetries, dimensionality, and conservation laws rather than microscopic details.

[1] B. D. Paulsen, K. Tybrandt, E. Stavrinidou, and J. Rivnay, Organic mixed ionic–electronic conductors, Nature materials **19**, 13 (2020).

[2] J. T. Friedlein, R. R. McLeod, and J. Rivnay, Device physics of organic electrochemical transistors, Organic Electronics **63**, 398 (2018).

[3] J. Rivnay, S. Inal, A. Salleo, R. M. Owens, M. Berggren, and G. G. Malliaras, Organic electrochemical transistors, Nat. Rev. Mater. **3**, 17086 (2018).

[4] T. He and C. D. Frisbie, Sub-band filling, mott-like transitions, and ion size effects in c60 single crystal electric double layer transistors, ACS nano **16**, 4823 (2022).

[5] D. H. Tjhe, X. Ren, I. E. Jacobs, G. D'avino, T. B. Mustafa, T. G. Marsh, L. Zhang, Y. Fu, A. E. Mansour, A. Opitz, *et al.*, Non-equilibrium transport in polymer mixed ionic–electronic conductors at ultrahigh charge densities, Nature Materials **23**, 1712 (2024).

[6] K. Xu, T.-P. Ruoko, M. Shokrani, D. Scheunemann, H. Abdalla, H. Sun, C.-Y. Yang, Y. Puttisong, N. B. Kolhe, J. S. M. Figueroa, *et al.*, On the origin of seebeck coefficient inversion in highly doped conducting polymers, Advanced Functional Materials **32**, 2112276 (2022).

[7] L. M. Bongartz, G. LeCroy, T. J. Quill, N. Siemons, G. Dijk, A. Marks, C. Cheng, H. Kleemann, K. Leo, and A. Salleo, Electron-ion coupling breaks energy symmetry in organic electrochemical transistors, arXiv preprint arXiv:2412.07921 (2024).

[8] M. Koopmans, M. A. Leiviskaä, J. Liu, J. Dong, L. Qiu, J. C. Hummelen, G. Portale, M. C. Heiber, and L. J. A. Koster, Electrical conductivity of doped organic semiconductors limited by carrier–carrier interactions, ACS Applied Materials & Interfaces **12**, 56222 (2020).

[9] X. Ji, B. D. Paulsen, G. K. Chik, R. Wu, Y. Yin, P. K. Chan, and J. Rivnay, Mimicking associative learning using an ion-trapping non-volatile synaptic organic electrochemical transistor, Nature communications **12**, 2480 (2021).

[10] S. Wang, X. Chen, C. Zhao, Y. Kong, B. Lin, Y. Wu, Z. Bi, Z. Xuan, T. Li, Y. Li, *et al.*, An organic electrochemical transistor for multi-modal sensing, memory and processing, Nature Electronics **6**, 281 (2023).

[11] K.-H. Choi, S. Im, A. Plant, C. Neri Soto, H. Lee, C. Choi, H. W. Jang, J. H. Cho, H. Ju, Y. Lee, *et al.*, Role of amorphous phases in mixed conduction of conjugated regioblock copolymers for organic electrochemical synaptic transistors, Advanced Materials , e02133 (2025).

[12] R. Wu, D. Meli, J. Strzalka, S. Narayanan, Q. Zhang, B. D. Paulsen, J. Rivnay, and C. J. Takacs, Bridging length scales in organic mixed ionic–electronic conductors through internal strain and mesoscale dynamics, Nature materials **23**, 648 (2024).

[13] L. M. Bongartz, R. Kantelberg, T. Meier, R. Hoffmann, C. Matthus, A. Weissbach, M. Cucchi, H. Kleemann, and K. Leo, Bistable organic electrochemical transistors: enthalpy vs. entropy, Nature Communications **15**, 6819 (2024).

[14] R. Ghosh and F. C. Spano, Excitons and polarons in organic materials, Accounts of Chemical Research **53**, 2201 (2020).

[15] L. M. Bongartz, A simulation tool is avaialbe on GitHub, `https://github.com/lukasbongartz/rust-lattice-simulator` (2025).

APPENDIX

Derivation of the Mean-Field Entropy

This appendix details the derivation of the entropy term used in the mean-field analysis, which appears in Eq. (5). The goal is to find an analytical expression for the configurational entropy S of a macrostate defined by a carrier density ρ.

The entropy arises from the number of ways, Ω, to arrange $N = \rho V$ indistinguishable charge carriers on a lattice of V distinguishable sites. This is a classic combinatorial problem, and the number of microstates is given by the binomial coefficient:

$$\Omega = \binom{V}{N} = \frac{V!}{N!(V-N)!} \tag{9}$$

The configurational entropy is the natural logarithm of this quantity:

$$S = \ln(\Omega) = \ln(V!) - \ln(N!) - \ln((V-N)!) \tag{10}$$

For a macroscopic system, V, N, and $(V-N)$ are all very large numbers, making the direct computation of the factorials impossible. We can, however, use Stirling's approximation for the natural logarithm of a factorial, which for large n is given by:

$$\ln(n!) = n\ln(n) - n + O(\ln(n)) \tag{11}$$

where $O(\ln(n))$ represents terms that grow on the order of $\ln(n)$. Applying this more accurate approximation to each term in the entropy equation yields:

$$\begin{aligned} S \approx & (V\ln V - V) - (N\ln N - N) \\ & - ((V-N)\ln(V-N) - (V-N)) \\ & + O(\ln V) - O(\ln N) - O(\ln(V-N)) \end{aligned} \tag{12}$$

The expression simplifies to:

$$S \approx V\ln V - N\ln N - (V-N)\ln(V-N) + O(\ln V) \tag{13}$$

where we have combined the logarithmic error terms, as they are all of the same order. We now express N in terms of the density $\rho = N/V$, so $N = \rho V$.

$$S \approx V\ln V - (\rho V)\ln(\rho V) - (V-\rho V)\ln(V-\rho V) + O(\ln V) \tag{14}$$

$$\begin{aligned} S \approx & V\ln V - \rho V(\ln\rho + \ln V) \\ & - (1-\rho)V(\ln(1-\rho) + \ln V) + O(\ln V) \end{aligned} \tag{15}$$

Expanding and grouping the terms involving $\ln V$:

$$\begin{aligned} S \approx & (V - \rho V - (1-\rho)V)\ln V \\ & - V\left(\rho\ln\rho + (1-\rho)\ln(1-\rho)\right) + O(\ln V) \end{aligned} \tag{16}$$

The prefactor for the leading $\ln V$ term is $V - \rho V - V + \rho V = 0$. This leaves us with the final expression for the entropy:

$$S \approx -V\left(\rho\ln\rho + (1-\rho)\ln(1-\rho)\right) + O(\ln V) \tag{17}$$

In the exponent of Eq. (5), this entropy term is combined with the energy term, which scales linearly with V. In the thermodynamic limit ($V \to \infty$), the $O(\ln V)$ term becomes negligible compared to the leading $O(V)$ terms. We can therefore safely neglect it to arrive at the entropy density, $s = S/V$:

$$s = \frac{S}{V} \approx -\left(\rho\ln\rho + (1-\rho)\ln(1-\rho)\right) \tag{18}$$

This is the standard expression for the entropy of mixing, which forms the entropic part of the mean-field free energy density in Eq. (5).